Raman dissipative soliton source of ultrashort pulses in NIR-III spectral window

INNOKENTIY ZHDANOV,[1,2,†]* [ID] VITALI M. VOLOSI,[1,3,†] NATALIA A. KOLIADA,[1,3,4] DENIS S. KHARENKO,[1,3] [ID] NAZAR A. NIKOLAEV,[1] SERGEI K. TURITSYN,[5] [ID] AND SERGEY A. BABIN[1,3] [ID]

[1]*Institute of Automation and Electrometry SB RAS, 1 Ac. Koptyug Ave., Novosibirsk, Russia*
[2]*Now with Institute of Photonics and Quantum Electronics (IPQ), Karlsruhe Institute of Technology (KIT), Karlsruhe, Germany*
[3]*Novosibirsk State University, 1 Pirogova Str., Novosibirsk, Russia*
[4]*Institute of Laser Physics SB RAS, 15 Ac. Lavrentiev Ave., Novosibirsk, Russia*
[5]*Aston Institute of Photonic Technologies, Aston University, Birmingham B4 7ET, UK*
[†]These authors contributed equally to this work
*zhdanovis@iae.nsk.su

Abstract: We present a novel fiber source of ultrashort pulses at the wavelength of 1660 nm based on the technique of external cavity Raman dissipative soliton generation. The output energy of the generated 30 ps chirped pulses is in the range of 0.5–3.6 nJ with a slope efficiency of 57%. Numerical simulations are in excellent agreement with the experimental results and the shape of the compressed pulses. The compressed pulses consist of a central part with a duration of 300 fs and a weak pedestal. Our results clearly demonstrate the potential to extend the spectral range of the Raman-assisted technique for generating ultra-short pulses to new frequency regions, including biomedical windows. This paves the way for the development of new dissipative soliton sources in these bands.

1. Introduction

Generation of an ultrashort optical pulse in the second water transparency window (1600–1700 nm) [1,2] and extended NIR-III (1550–1800 nm) [3] spectral region is in demand due to various biomedical applications, including multi-photon fluorescence microscopy [4,5], optical coherent tomography [6], and coherent anti-Stokes [7] and stimulated Raman spectroscopy [8]. Pulse generation in the 1600-1700 nm range can be done by either using active medium-based lasers or frequency converters, and both approaches have corresponding specific challenges.

Direct generation became possible due to the recent advances in thulium [9,10], thulium-holmium [11], and bismuth doped active fibers [12–14]. One of the main challenges in the thulium fiber laser emitting radiation around 1700 nm wavelength range was to overcome the high ground state absorption [15] and suppress the amplified spontaneous emission (ASE) at wavelengths above 1800 nm [10]. The tunable thulium laser mode-locked via nonlinear polarization evolution (NPE) with inserted photonic crystal fiber for long-wavelength ASE suppression was developed [10]. The amplified pulses had a duration of 2.55 ps at 1725 nm, however, their energy level was not discussed. Another example of a short wavelength mode-locked thulium-doped fiber system based on the amplification of conventional solitons was made by Li where pulses with 445 fs duration and 5.7 nJ energy at 1785 nm have been demonstrated [9]. Recent results include a net-normal dispersion master oscillator and specially designed W-shape thulium-doped active fiber [16]. In [17] Nonlinear amplifying loop mirror (NALM)-based mode-locked laser with this special fiber demonstrated 0.8 nJ pulse energy at 4.96 MHz repetition rate in stretched pulse

regime at the wavelength of 1785 nm. Further amplification of the pulses using the same fiber resulted in a 158.2 nJ energy. However, the best-quality compressed pulses were obtained for the seed with a small net dispersion, leading to an energy of 128 nJ and pulse duration of 174 fs. Interesting results have been demonstrated in [11] in a thulium-holmium fiber laser incorporating an acoustic-optical modulator-based spectral filter. In this laser configuration, they successfully achieved widely-tunable soliton generation spanning over 100 nm, with a pulse duration of 630 fs. However, it should be noted that this required a pump power of 1-2 watts and exhibited extremely low conversion efficiency.

Besides thulium-doped fibers, direct pulse generation in a target wavelength range was demonstrated using special bismuth fibers [12,13,18] developed by the Fiber Optics Research Center of RAS. In [19], pulse generation was achieved in a linear cavity using a carbon nanotube saturable absorber in both anomalous and normal dispersion regimes. The generated pulses exhibited duration of 1.65 ps for solitons and 14 ps for chirped normal dispersion pulses, which could be subsequently compressed down to 1.2 ps. This study showcased the versatility of the carbon nanotube saturable absorber in generating a range of pulse characteristics. In another work pulse generation was demonstrated in a NALM-mode-locked fiber cavity operating at a wavelength of 1.7 µm [14]. The generated dissipative solitons exhibited an energy of 84 pJ and a duration of 17.7 ps. After amplification, the energy of the pulses increased to 5.7 nJ, demonstrating the capability for significant pulse energy scaling.

Nonlinear frequency conversion, such as optical parametric oscillators (OPO) or stimulated Raman scattering (SRS)-based light sources, offers an interesting alternative to direct emitting lasers. In [20] it was presented a tunable fiber OPO pumped with chirped dissipative solitons. The OPO exhibited a remarkable tunability range for the idler wave, spanning from 1620 nm to 1870 nm. The pulse energy achieved nJ-level at 1670 nm. The pump-to-idler conversion efficiency was measured at 20%. The ultrashort pulse generation at 1700 nm with 22% efficiency using the pre-designed idler wave was demonstrated in [2]. The average power reached 1.42 W, corresponding to a pulse energy of 40 nJ. These pulses could be dechirped using a grating compressor, resulting in a duration of 450 fs and a peak power of 55 kW.

Various techniques utilizing frequency conversion via SRS have been explored, including soliton self-frequency shift [21–24], Raman pulse generation [25,26], and Raman dissipative soliton (RDS) generation [27,28]. Of particular interest is the Raman self-frequency shift technique in [24]. By employing a specially designed large-mode area anti-resonant fiber, the generation of 85 fs pulses with peak powers of 983 kW at 1800 nm and 725 kW at 1680 nm has become achievable. Another significant aspect of this work is the utilization of the generated 1680 nm pulses for a three-photon nonlinear microscopy experiment, where only 8 mW of the potential 70 mW was used to illuminate the sample. This highlights the efficient and effective bio-medical application of the generated pulses.

Note, that the RDS method requires feedback, which can be implemented through either an internal cavity in the master oscillator [27] or synchronous pumping of an external cavity [28,29]. These techniques have been successfully applied in Ytterbium fiber lasers to generate ultrashort pulses at the Raman-shifted wavelength, with durations in the range of several hundred femtoseconds and energies reaching up to tens of nJ. The use of an Erbium fiber laser for pumping presents an opportunity to produce ultrashort pulses in the NIR-III spectral region. Notably, in [30], a tunable generation of Raman pulses in the range of 1702.6–1728.84 nm was demonstrated by synchronously pumping with dissipative solitons, achieving a slope efficiency of 35.79%. However, the pulse duration in this case was approximately 4.3 ps, and the pulse energy did not exceed 1 nJ [30].

In this paper, we demonstrate for the first time, to the best of our knowledge, Raman dissipative soliton generation through an all-fiber external cavity synchronously pumped by an Erbium-doped mode-locked fiber laser. The experimental results are in good agreement with our numerical

modeling. Furthermore, we assessed the quality and coherency of the obtained RDSs by compressing them in a standard single-mode fiber, achieving a duration of 300 fs at the carrier wavelength of 1660 nm.

2. Experimental setup

The developed system consists of three parts, depicted in Fig. 1: seed mode-locked laser (MLL), chirped-pulse amplifier (CPA), and external cavity. The MLL is an NPE mode-locked Erbium fiber laser with a net-normal ring cavity operating in a highly-chirped dissipative soliton (HCDS) regime, presented previously in [31]. A filter based on a bulk diffraction grating and a dual-fiber collimator provides the clean Gaussian spectral shape required for the HCDS generation in a net normal dispersion cavity and a small tuning of the repetition rate required for exact matching of the seed and external cavity lengths. The seed provides 0.6 mW average power of the pulse train with a repetition rate of 6.54 MHz at the 30% coupler output placed just before the spectral filter. We use an intracavity pulse from the coupler output for further amplification as it has a more homogeneous optical spectrum than a pulse from an NPE rejection output port.
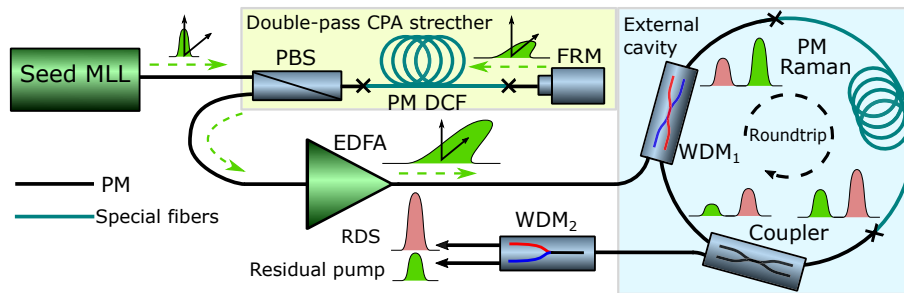

Fig. 1. Scheme of Raman Dissipative Soliton (RDS) generator by the synchronous pump of the external cavity: MLL — mode-locked laser, PBS — polarization beam splitter, DCF — dispersion compensating fiber, FRM — Faraday rotator mirror, EDFA — Erbium-doped fiber amplifier, WDM — wavelength division multiplexer.

The second part complements the first one and represents a commercial optical fiber amplifier (Erbius, TekhnoScan) with a CPA scheme. The stretcher was a polarization-maintaining (PM) optical fiber with a high normal dispersion of 128 ± 12 ps^2/km (Thorlabs PMDCF), polarization beam splitter (PBS), and Faraday rotator mirror (FRM). FRM was used to implement the second pass through Thorlabs PMDCF, which effectively doubles the length of the stretch by rotating the polarization in $\pi/2$ on reflection and provides additional pulse broadening before amplification. To separate different polarizations, we used PBS before the stretcher. The total dispersion of the stretcher was estimated at 1.6 ps^2. Finally, we were able to achieve an amplification up to 180 mW (27 nJ) at 1.55 μm carrier wavelength. Resulted spectral shape is presented in Fig. 2(a) (left).

The master oscillator and the amplifier form the pump pulse source for the RDS generation in the external ring cavity. It includes a PM 1550/1620 nm WDM followed by 26.8 meters of 5/125 high Raman gain PM fiber (PM Raman, OFS) and a PM 80/20 fused coupler. The external cavity length was varied to maximize the coincidence of the seed MLL and external cavities bypassed frequencies for RDS generation. Fine-tuning was carried out by changing the length of the seed laser cavity by varying the distance between the dual-fiber collimator and the diffraction grating with sub-μm accuracy. Pulse characterization has been performed by an optical spectral analyzer (OSA, Yokogawa 6370), frequency-resolved optical gating (FROG) system (Mesaphotonics Ltd.), radio frequency (RF) analyzer (Agilent N9010A) and Thorlabs power meter.
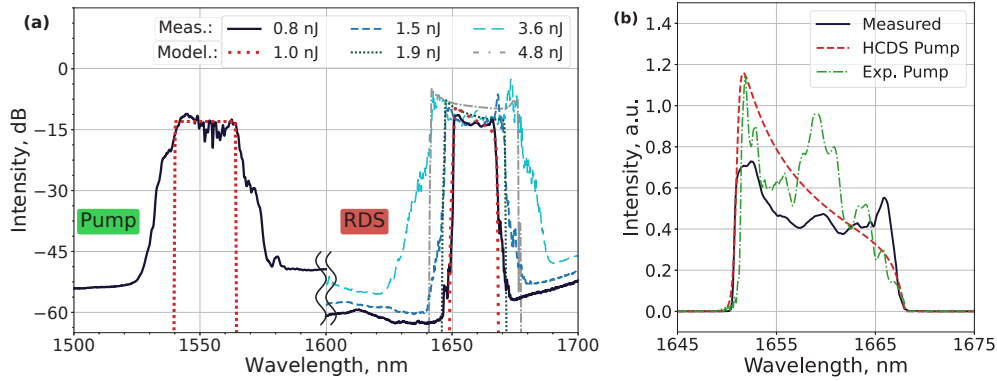
Fig. 2. (a) Correspondence of the measured and the model pump spectra (left) and comparison of the measured and calculated RDS spectra at the different pulse energies (right). (b) Comparison of the measured optical spectrum of the RDS with the calculated ones obtained for the analytical and experimental pump shapes in linear scale.

3. Numerical simulation

We performed numerical simulations to gain insight into the operation of the studied Raman laser and investigate the effect of varying operating parameters on the temporal shape and optical spectrum of the generated pulses. It was based on solving the nonlinear Schrödinger equation (NLSE) of pulse propagation through the optical fibers in the Raman laser cavity [32] using the *PyOFSS* [33] library and considering the Raman response function based on the multiple-vibrational-mode model for the silica fiber [34]. For a pump pulse, the analytical expression for HCDS [35] was chosen:

$$A(z, t) = \sqrt{P} \operatorname{sech}^{1+iC}(t/t_p) \exp(i\phi z), \tag{1}$$

where P is the peak power of the pulse, C — chirp parameter, t_p — pulse duration. The values of C and t_p were chosen to be consistent with the experimental: 100 rad and 18.8 ps (full width at half maximum), respectively. The correspondence of the chirp parameter was determined by the spectrum width with the fixed pulse duration (see Fig. 2(a) on the left). The peak power was varied to match the simulated and experimental RDSs spectra (the right part of Fig. 2(a)). To investigate the fine structure of an RDS spectrum, we also simulate the initial pump pulse based on adding proper chirp to the measured pump spectrum (see Fig. 2(b)). As a result, additional peaks appear in exactly the same place as in the experiment but with a slightly different amplitude. Since there is no significant difference, we will use the analytical expression for the pump pulses in all further calculations.

The simulated scheme corresponds to the experimental one and is depicted in Fig. 3. The initial point is on the WDM, where the pump pulse starts to propagate in the external cavity. It includes optical fibers with anomalous (PM1550) and normal (PM Raman) dispersion values of (-22 ps²/km and 26 ps²/km correspondingly). The nonlinearity values were estimated as 2 and 7 $(W \cdot km)^{-1}$. At the output coupler, a loss of 80% is applied. Such value was determined as the most appropriate to obtain high-quality RDSs with elements available in the experiment. A linear time delay followed next is necessary to match a generated Raman pulse with the pump pulse at a new roundtrip. Delay variation allows us to tune a carrier wavelength of RDSs and match it with the experimental one. The output pulse is taken from the coupler input and additional losses which correspond to its ratio of 20% and further elements of 0.55 dB are applied to calculate output energy values, presented in Fig. 2(a). As a result, almost quantitative agreement between the simulation and the experiment was obtained for a set of points (see Fig. 2(a) on the right).

Numerical compression was performed in a piece of PM1550 fiber and will be compared with the experiment further.
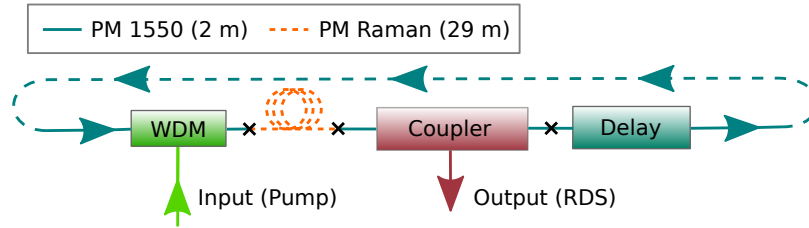

Fig. 3. Representation of the external cavity used in the numerical simulation.

4. Experimental results

A generation of stable RDSs in the experiment is set as soon as the repetition rates are matched and sufficient power of the pump pulses is reached. Pulse spectral shape depicted in Fig. 2(a) (right) allows us to conclude that obtained pulses are truly HCDS [36] with the carrier wavelength of 1.66 μm. The dependence of the RDS power is linear, which is typical for Raman fiber lasers. The threshold is only 5 mW (0.8 nJ), and the slope efficiency is 57% (see green dashed line in Fig. 4(a)). The power of the generated pulses varies from 3.6 to 23.8 mW, which corresponds to a pulse energy of 0.5–3.6 nJ. The maximal energy was limited by the transition to a noise-like pulse generation regime. The optical spectrum width grows proportionally to a pulse power (see right axis in Fig. 4(a)) up to 35 nm (−10 dB level). Such behavior is consistent with the previous work [28,37] where Yb-doped fiber MLL was used as a pump. The radio frequency spectrum of RDS shows a high signal-to-noise ratio of 60 dB and is presented in Fig. 4(b). The pulse repetition rate is 6.54 MHz, which coincides with the pulse repetition rate of the pump laser.
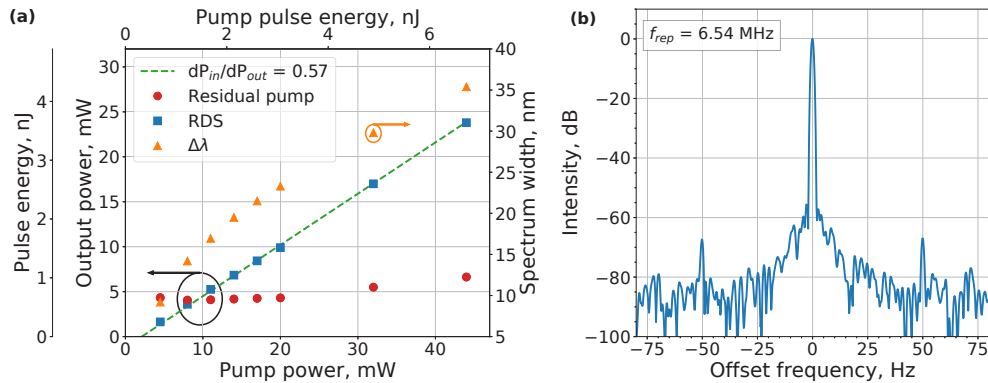

Fig. 4. (a) The RDS power (blue squares related to the left axis) and the optical spectrum width (at −10 dB level, orange triangles related to the right axis) as a function of pump power. The residual pump power is also presented by red circles. Corresponding pulse energy values are presented on the additional left and top axes. (b) RF spectrum of the generated RDSs, centered at the repetition rate of 6.54 MHz.

    To demonstrate a high coherence of obtained RDS, we performed its compression in a piece of fiber with anomalous dispersion (55 meters of PM1550). The initial chirped pulse duration was about 30 ps. By varying the pump pulse power, we could achieve the most effective compression for RDS with 5.2 mW average power (0.8 nJ energy). A comparison of obtained experimental

results with the numerical compression simulation is shown in Fig. 5. The measured FROG-trace was retrieved by using the *pyret* library [38] to extract a temporal shape. It was used to calculate the retrieved FROG-trace, which demonstrates an agreement with the measured one (see Fig. 5(a)) and proves the correction of the retrieval procedure. Figure 5(b) shows the optical spectra retrieved from the FROG-trace, measured by OSA and obtained from the numerical compression simulation. As it can be seen, all spectra match each other with high accuracy. Finally, the retrieved and simulated temporal shapes are shown in Fig. 5(c). It is important to note that the calculated temporal shape reproduces well not only the central part but also the pedestal, which indicates a high reliability of the developed numerical model. In addition, that also means that it can be used further for a complex optimization of compressor configuration to improve the performance of RDS generator in terms of clear temporal shape, shorter duration, and high pulse energy. The resulting compressed pulse duration is 300 fs with a central wavelength of 1660 nm and a peak power of almost 1.5 kW. RDS with higher energy rapidly degraded or split into sub-pulses due to the high nonlinear phase accumulation in the fiber. This effect can be mitigated by using a diffraction-grating-based compressor instead of the fiber one. To prove this statement, we numerically investigated a potential improvement of compressed pulse peak power. We launched a 4.8 nJ energy pulse which is comparable with the level reached experimentally (see Fig. 4(a)) and simulated its compression during propagation in a diffraction grating compressor with compensated β_2 and β_3 (green-dashed line, Fig. 5(c)). Unfortunately, we can not provide experimental results due to the limitation of our setup, but our numerical simulation demonstrated a potential possibility for further peak power increase to 6 kW with a comparable dechirped pulse duration. It should also be noted that further energy up-scaling can be achieved by using fiber amplifiers based on Bismuth-doped fibers, Raman effect, or parametric processes. The specific realization can become a point of separate investigations.
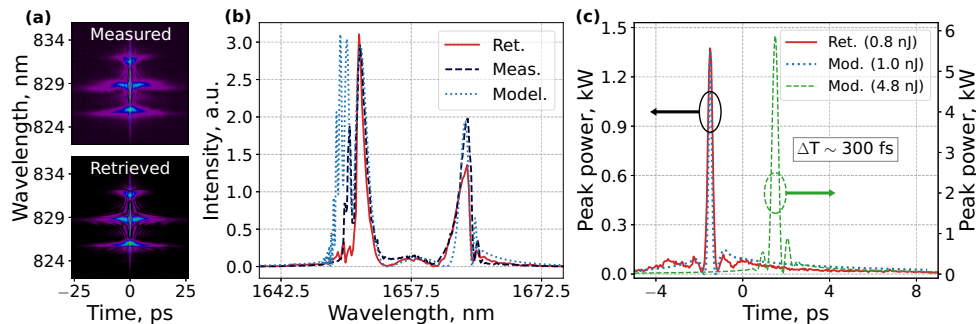

Fig. 5. A complete comparison of the measured, retrieved, and calculated data, including FROG-traces (a), optical spectra (b), and the temporal shape of the compressed RDS (c).

5. Conclusion

The work successfully demonstrated, for the first time, the generation of Raman dissipative solitons (RDSs) in the vicinity of 1.7 μm through synchronous pumping of an external cavity using an Erbium-doped mode-locked fiber laser. Both experimental and numerical investigations were conducted to study the dependence of RDS parameters on the energy of the pumping pulses. This comprehensive analysis provided valuable insights into the behavior and characteristics of RDSs under different pumping conditions. By performing numerical simulations, the most effective and easily implementable configuration for the external cavity was identified, with a feedback value of 20%. This finding has practical significance and can guide the design and optimization of RDS generation setups.

We achieved a pump-to-RDS slope efficiency of 57% at the carrier wavelength of 1660 nm and an energy output ranging from 0.5 to 3.6 nJ. To demonstrate the feasibility of compression, a simple proof-of-principle scheme was employed, leading to the generation of ultrashort pulses with a duration of 300 fs and a peak power of nearly 1.5 kW. This successful compression process highlights the potential for obtaining high-intensity, short-duration pulses using the stimulated Raman scattering effect. The peak power improvement up to the level required by applications seems to be achievable with a combination of the optimized compressor and an amplifier. From a fundamental scientific standpoint, this work establishes that stimulated Raman scattering is a versatile and universal method for generating ultrashort pulses at any desired wavelength, catering to various application requirements. Furthermore, it opens up opportunities for further exploration of Raman-assisted operating modes, such as the generation of stretched or self-similar pulses within an external cavity. Moreover, this compact and reliable fiber source holds great promise for applications in nonlinear biomedical imaging, particularly in the NIR-III window. The combination of these features makes it highly suitable for advancing nonlinear imaging techniques in the field of biomedical research.

Disclosures. The authors declare no conflicts of interest.

Data availability. Data underlying the results presented in this paper are not publicly available at this time but may be obtained from the authors upon reasonable request. The realized numerical model is available on the PyOFSS website [33] in the examples folder.

References

1. C. Xu and F. W. Wise, "Recent advances in fibre lasers for nonlinear microscopy," Nat. Photonics **7**(11), 875–882 (2013).
2. Y. Qin, O. Batjargal, B. Cromey, and K. Kieu, "All-fiber high-power 1700 nm femtosecond laser based on optical parametric chirped-pulse amplification," Opt. Express **28**(2), 2317–2325 (2020).
3. T.-M. Liu, J. Conde, T. Lipiński, A. Bednarkiewicz, and C.-C. Huang, "Revisiting the classification of nir-absorbing/emitting nanomaterials for in vivo bioapplications," NPG Asia Mater. **8**(8), e295 (2016).
4. W. R. Zipfel, R. M. Williams, and W. W. Webb, "Nonlinear magic: multiphoton microscopy in the biosciences," Nat. Biotechnol. **21**(11), 1369–1377 (2003).
5. M. Yamada, L. L. Lin, and T. W. Prow, "Multiphoton Microscopy Applications in Biology," in *Fluoresc. Microsc.* (Elsevier, 2014), pp. 185–197.
6. S. P. Chong, C. W. Merkle, D. F. Cooke, T. Zhang, H. Radhakrishnan, L. Krubitzer, and V. J. Srinivasan, "Noninvasive, in vivo imaging of subcortical mouse brain regions with 1.7 μm optical coherence tomography," Opt. Lett. **40**(21), 4911 (2015).
7. S. Roy, J. R. Gord, and A. K. Patnaik, "Recent advances in coherent anti-Stokes Raman scattering spectroscopy: Fundamental developments and applications in reacting flows," Prog. Energy Combust. Sci. **36**(2), 280–306 (2010).
8. C. W. Freudiger, W. Yang, G. R. Holtom, N. Peyghambarian, X. S. Xie, and K. Q. Kieu, "Stimulated Raman scattering microscopy with a robust fibre laser source," Nat. Photonics **8**(2), 153–159 (2014).
9. C. Li, X. Wei, C. Kong, S. Tan, N. Chen, J. Kang, and K. K. Y. Wong, "Fiber chirped pulse amplification of a short wavelength mode-locked thulium-doped fiber laser," APL Photonics **2**(12), 121302 (2017).
10. S. D. Emami, M. M. Dashtabi, H. J. Lee, A. S. Arabanian, and H. A. A. Rashid, "1700 nm and 1800 nm band tunable thulium doped mode-locked fiber lasers," Sci. Rep. **7**(1), 12747 (2017).
11. T. Noronen, O. Okhotnikov, and R. Gumenyuk, "Electronically tunable thulium-holmium mode-locked fiber laser for the 1700-1800 nm wavelength band," Opt. Express **24**(13), 14703 (2016).
12. S. Firstov, S. Alyshev, M. Melkumov, K. Riumkin, A. Shubin, and E. Dianov, "Bismuth-doped optical fibers and fiber lasers for a spectral region of 1600–1800 nm," Opt. Lett. **39**(24), 6927 (2014).
13. S. V. Firstov, S. V. Alyshev, K. E. Riumkin, A. M. Khegai, A. V. Kharakhordin, M. A. Melkumov, and E. M. Dianov, "Laser-Active Fibers Doped with Bismuth for a Wavelength Region of 1.6-1.8 μm," IEEE J. Sel. Top. Quantum Electron. **24**(5), 1–15 (2018).
14. A. Khegai, M. Melkumov, K. Riumkin, V. Khopin, S. Firstov, and E. Dianov, "NALM-based bismuth-doped fiber laser at 1.7 μm," Opt. Lett. **43**(5), 1127–1130 (2018).

15. P. Peterka, I. Kasik, A. Dhar, B. Dussardier, and W. Blanc, "Theoretical modeling of fiber laser at 810 nm based on thulium-doped silica fibers with enhanced $^3H_4$ level lifetime," Opt. Express **19**(3), 2773 (2011).

16. S. Chen, Y. Chen, K. Liu, R. Sidharthan, H. Li, C. J. Chang, Q. J. Wang, D. Tang, and S. Yoo, "All-fiber short-wavelength tunable mode-locked fiber laser using normal dispersion thulium-doped fiber," Opt. Express **28**(12), 17570 (2020).

17. S. Chen, Y. Chen, K. Liu, R. Sidharthan, H. Li, C. J. Chang, Q. J. Wang, D. Tang, and S. Yoo, "W-type normal dispersion thulium-doped fiber-based high-energy all-fiber femtosecond laser at 1.7 μm," Opt. Lett. **46**(15), 3637 (2021).

18. E. M. Dianov, "Bismuth-doped optical fibers: a challenging active medium for near-ir lasers and optical amplifiers," Light: Sci. Appl. **1**(5), e12 (2012).

19. T. Noronen, S. Firstov, E. Dianov, and O. G. Okhotnikov, "1700 nm dispersion managed mode-locked bismuth fiber laser," Sci. Rep. **6**(1), 24876 (2016).

20. M. Tang, R. Becheker, P.-H. Hanzard, A. Tyazhev, J.-L. Oudar, A. Mussot, A. Kudlinski, T. Godin, and A. Hideur, "Low noise high-energy dissipative soliton erbium fiber laser for fiber optical parametric oscillator pumping," Appl. Sci. **8**(11), 2161 (2018).

21. T. N. Nguyen, K. Kieu, D. Churin, T. Ota, M. Miyawaki, and N. Peyghambarian, "High Power Soliton Self-Frequency Shift With Improved Flatness Ranging From 1.6 to 1.78 μm," IEEE Photonics Technol. Lett. **25**(19), 1893–1896 (2013).

22. L. Kotov, M. Likhachev, M. Bubnov, D. Lipatov, A. Guryanov, M. Tang, A. Hideur, and S. Février, "1700-nm High-Energy All-Fiber Format Femtosecond Laser," in *2015 European Conference on Lasers and Electro-Optics - European Quantum Electronics Conference*, (Optical Society of America, 2015).

23. P. Cadroas, L. Abdeladim, and L. Kotov, *et al.*, "All-fiber femtosecond laser providing 9 nj, 50 mhz pulses at 1650 nm for three-photon microscopy," J. Opt. **19**(6), 065506 (2017).

24. H. Delahaye, C.-H. Hage, S. M. Bardet, I. Tiliouine, G. Granger, D. Gaponov, L. Lavoute, M. Jossent, S. Aleshkina, M. Bubnov, M. Salganskii, D. Lipatov, A. Guryanov, M. Likhachev, F. Louradour, and S. Février, "Generation of megawatt soliton at 1680 nm in very large mode area antiresonant fiber and application to three-photon microscopy," J. Opt. **23**(11), 115504 (2021).

25. A. Gladyshev, M. Astapovich, Y. Yatsenko, A. Kosolapov, A. Okhrimchuk, and I. Bufetov, "SRS generation of femtosecond pulses in a methane-filled revolver hollow-core optical fibre," Quantum Electron. **49**(12), 1089–1092 (2019).

26. W. Qi, J. Zhou, S. Cui, X. Cheng, X. Zeng, and Y. Feng, "Femtosecond Pulse Generation by Nonlinear Optical Gain Modulation," Adv. Photonics Res. **3**(3), 2100255 (2022).

27. S. A. Babin, E. V. Podivilov, D. S. Kharenko, A. E. Bednyakova, M. P. Fedoruk, V. L. Kalashnikov, and A. Apolonski, "Multicolour nonlinearly bound chirped dissipative solitons," Nat. Commun. **5**(1), 4653 (2014).

28. D. Churin, J. Olson, R. A. Norwood, N. Peyghambarian, and K. Kieu, "High-power synchronously pumped femtosecond raman fiber laser," Opt. Lett. **40**(11), 2529–2532 (2015).

29. A. E. Bednyakova, D. S. Kharenko, I. Zhdanov, E. V. Podivilov, M. P. Fedoruk, and S. A. Babin, "Raman dissipative solitons generator near 1.3 mkm: limiting factors and further perspectives," Opt. Express **28**(15), 22179–22185 (2020).

30. H. Yang, R. Zhang, X. Jiang, J. Evans, and S. He, "1.7 μm - 1.73 μm tunable ultrafast raman fiber laser pumped by 1.6 μm dissipative soliton pulses," Opt. Express **30**(25), 45970 (2022).

31. I. S. Zhdanov, A. E. Bednyakova, V. M. Volosi, and D. S. Kharenko, "Energy scaling of an erbium-doped mode-locked fiber laser oscillator," OSA Continuum **4**(10), 2663 (2021).

32. A. E. Bednyakova, S. A. Babin, D. S. Kharenko, E. V. Podivilov, M. P. Fedoruk, V. L. Kalashnikov, and A. Apolonski, "Evolution of dissipative solitons in a fiber laser oscillator in the presence of strong Raman scattering," Opt. Express **21**(18), 20556–20564 (2013).

33. D. S. Kharenko, "Pyofss: Python-based optical fibre system simulator," Github (2022) https://github.com/galilley/pyofss.

34. D. Hollenbeck and C. D. Cantrell, "Multiple-vibrational-mode model for fiber-optic Raman gain spectrum and response function," J. Opt. Soc. Am. B **19**(12), 2886–2892 (2002).

35. S. K. Turitsyn, N. N. Rozanov, I. A. Yarutkina, A. E. Bednyakova, S. Fedorov, O. V. Shtyrina, and M. P. Fedoruk, "Dissipative solitons in fiber lasers," Usp. Fiz. Nauk **186**(7), 713–742 (2016).

36. D. S. Kharenko, O. V. Shtyrina, I. A. Yarutkina, E. V. Podivilov, M. P. Fedoruk, and S. A. Babin, "Highly chirped dissipative solitons as a one-parameter family of stable solutions of the cubic-quintic Ginzburg-Landau equation," J. Opt. Soc. Am. B **28**(10), 2314–2319 (2011).

37. D. S. Kharenko, V. D. Efremov, and S. A. Babin, "Study on harmonic generation regimes of Raman dissipative solitons in an external fibre cavity in a spectral region of 1.3 μm," Quantum Electron. **49**(7), 657–660 (2019).

38. N. C. Geib, M. Zilk, T. Pertsch, and F. Eilenberger, "Common pulse retrieval algorithm: a fast and universal method to retrieve ultrashort pulses," Optica **6**(4), 495 (2019).